Handle on the antiferromagnetic spin structure of NiO using a ferromagnetic adlayer

E. Heppell [1,2,3] F. Maccherozzi,[2] L. S. I. Veiga,[2] S. Langridge,[3] G. van der Laan [2] T. Hesjedal [1,2] and D. Backes [2]
[1]*Department of Physics, Clarendon Laboratory, University of Oxford, Oxford OX1 3PU, United Kingdom*
[2]*Diamond Light Source, Harwell Science and Innovation Campus, Didcot OX11 0DE, United Kingdom*
[3]*ISIS, Rutherford Appleton Laboratory, Harwell Science and Innovation Campus, Didcot OX11 0QX, United Kingdom*

(Received 30 September 2024; accepted 10 January 2025; published 27 January 2025)

Antiferromagnets (AFs) are characterized by spin structures that are resistant to external magnetic fields, rendering them ideal for persistent information storage but challenging to control. This study demonstrates that a thin ferromagnetic adlayer can serve as a magnetic 'lever' to provide a strong handle on the spin texture of an adjacent antiferromagnet. In bilayers composed of NiO(001) and Co, the expected exchange bias effect—a unidirectional shift in the Co hysteresis due to coupling with NiO—is notably absent. Instead, a strong interfacial coupling is observed, causing the NiO to partially follow the magnetization of Co under an applied magnetic field. Using x-ray magnetic linear dichroism, we detect an inversion of dichroism, indicating a reorientation of the Néel vector in NiO. X-ray spectromicroscopy imaging further reveals a direct correlation between ferromagnetic and antiferromagnetic domain structures. These findings are explained using a toy model that distinguishes between stable and unstable AF domains, highlighting the dynamic interplay between NiO and the Co adlayer in the presence of a magnetic field.

DOI: 10.1103/PhysRevMaterials.9.014408

I. INTRODUCTION

Antiferromagnets (AFs) have long been in the shadow of ferro- and ferrimagnets but have recently become the center of attention for both fundamental and applied condensed matter physics. The shift in focus is driven by the discovery of spin-orbit torques and magnetoresistance effects in AFs, which offer new means for measuring and controlling their spin structure [1]. Thus, a path toward AF spintronic devices has been paved, offering greater robustness against external magnetic fields and significantly faster switching speeds [2,3]. AFs consist of two ferromagnetically (FM) ordered sublattices that result in a virtually net zero magnetization. This has profound implications for their domain structure, which is dominated by exchange interactions, unlike ferromagnets, where both exchange and dipolar interactions play significant roles. However, accurately determining the spin structure of AFs remains challenging due to their zero or near-zero net magnetization, which lies well below the sensitivity limits of most magnetic characterization techniques.

The progress in understanding AFs can be exemplified by the extensive research on NiO. The material has been thoroughly studied using photoemission electron microscopy (PEEM) through both direct and indirect methods. Direct studies utilize x-ray magnetic linear dichroism (XMLD) to probe the spin structure [4–6], while indirect studies examine the effect of NiO on adjacent FMs using x-ray magnetic circular dichroism (XMCD) [7–9]. XMLD measurements have been conducted on both cleaved NiO single crystals [6,8,10,11] and thin films [12]. In contrast, combined XMCD/XMLD studies typically focus on NiO/ferromagnet bilayers, allowing for the exploration of interfacial interactions and coupling between the materials [13,14].

Recently, the influence of applied currents on the spin structure of NiO has been investigated using XMLD-PEEM imaging [15–23], providing complementary insights to those obtained from transport measurements [15,24–29]. While current-induced switching has been a key method for manipulating the AF spin structure [15–17,22,26–28,30], other approaches, such as laser excitation [20] and electric fields [31,32], have also proven effective in controlling NiO. Alongside these manipulation techniques, new methods for detecting the spin structure of AFs are rapidly developing. These include Lorentz transmission electron microscopy [33], spin-Seebeck imaging [34], THz spectroscopy [35–37], free-electron laser studies [38], resonant inelastic x-ray scattering [39], x-ray-detected ferromagnetic resonance [40], and grazing-incidence reflectivity [41,42].

Previous experiments focused mainly on NiO(111) with an in-plane Néel vector, exhibiting a strong exchange-bias effect of the NiO on the spin structure of an adjacent ferromagnet. In contrast, here we demonstrate the reverse effect: how a ferromagnet influences the less-studied NiO(001) with a canted Néel vector. Our results show that a Co adlayer provides a strong handle on the in-plane component of the Néel vector. Through XMLD spectroscopy and imaging, we demonstrate that applying relatively moderate magnetic fields can maximize and invert the spin structure of NiO. Notably, these magnetic fields have no effect on NiO when the adlayer is absent. Detailed XMLD-PEEM imaging reveals the spin

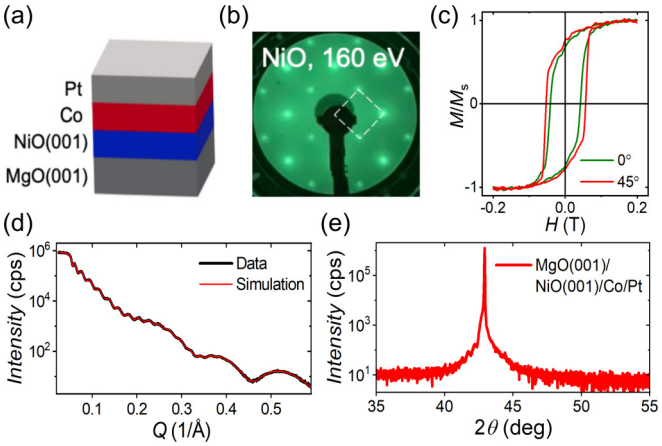

FIG. 1. (a) Schematic representation of the layer stack. (b) LEED pattern of the NiO(001) film on MgO(001). (c) Magnetic hysteresis curves, $M/M_S(H)$, with the magnetic field applied in two in-plane directions, along the [110] direction, i.e., $\phi = 0°$ (green curve), and along the [100] direction, i.e., $\phi = 45°$ (red curve). (d) XRR and (e) XRD measurements of the sample.

structure of NiO before and after the application of a magnetic field, providing valuable insights that enable us to develop a toy model describing the switching mechanism. Additionally, a principal component analysis (PCA) links the observed changes in the AF domains in PEEM to variations in the XMLD spectra. Our findings could lead to novel approaches to precisely control the spin structure of NiO by utilizing an FM adlayer, proving that XMLD imaging and spectroscopy can play an important role in the development of AF-based devices.

II. SAMPLE PREPARATION

NiO(001) layers with a thickness of 23 nm were deposited on MgO(001) substrates at a temperature of 430 °C using reactive DC magnetron sputtering from a Ni target. The MgO(001) substrates were preannealled at 1000 °C in air before sputtering. Ar and O_2 were used as the sputtering gases in a ratio of 9:2, with a total pressure of 2×10^{-2} mbar. The ultrahigh vacuum growth chamber has a base pressure of $<5\times10^{-8}$ mbar. Following deposition, the films were transferred *ex situ* from the oxide chamber to the metal chamber, which has a base pressure of $<4\times10^{-9}$ mbar. In the metal chamber using DC magnetron sputtering, the NiO layers were overgrown at room temperature with a 3-nm-thick polycrystalline Co layer, which is thick enough to exhibit in-plane anisotropy. A 1.5-nm-thick Pt capping layer was subsequently deposited to prevent oxidation.

A schematic of the heterostructure is shown in Fig. 1(a), along with the x-ray reflectivity (XRR) data in Fig. 1(d) (black curve), from which a model fit (red curve) was used to determine the layer thicknesses [43]: 22.7 nm for NiO, 2.8 nm for Co, and 1.5 nm for Pt. Figure 1(e) presents x-ray diffraction (XRD) data of the heterostructure, focusing on the region around the MgO(002) substrate peak. The much smaller NiO(002) peak is visible as a subtle shoulder on the MgO peak. The low-energy electron diffraction (LEED) data of the NiO(001) film on MgO(001) is presented in Fig. 1(b), showing the well-established (1×1) structure (marked by the dashed white square).

The AF crystalline anisotropy of NiO(001) deposited on MgO(001) results in four possible Néel vector orientations: [±5 ±5 19] [17]. These Néel vectors are canted 20° away from the sample normal, with their in-plane projections along the ⟨110⟩ crystallographic directions. The complex domain structure is a result of the compressive strain in the out-of-plane direction of the NiO layer [17].

The presence of AF in NiO was confirmed using XMLD, while the FM properties of the Co layer were verified using XMCD. To saturate the Co layer along its easy in-plane direction, magnetic fields were applied in the in-plane direction of the sample (x- and y-directions).

The sample holder was rotated to adjust the alignment of the x-rays, shifting from being perpendicular to the easy axis ($\theta = 0°$, measured relative to the surface normal) to nearly parallel ($\theta = 60°$). This adjustment ensured optimal contrast for magnetic measurements.

III. HYSTERESIS MEASUREMENTS

Figure 1(c) presents hysteresis loops measured using vibrating sample magnetometry (VSM). The magnetic field was applied in-plane with an angle ϕ with respect to the x direction, with $\phi = 0°$ (45°) aligned along the easy (hard) anisotropy direction of the AF [see Fig. 2(a)]. The coercivity observed in these measurements is significantly higher than that of a single Co layer—a characteristic often seen in exchange bias systems [44]. As expected, the coercivity of the Co layer is larger when the magnetic field is applied along the hard axis compared to the easy axis of NiO, as the magnetization reversal requires overcoming a greater energy barrier. However, an exchange bias field is either smaller than 0.5 mT or not present at all. The discrepancy in exchange bias observed at opposite orientations of the sample could result from training effects, but it is more likely further evidence supporting the absence of exchange bias.

Previous reports of exchange bias in NiO/Co bilayers primarily involve NiO(111) layers, where the Néel vector lies in-plane [45]. In contrast, no such effect has been reported for NiO(001), where the Néel vector is predominantly out-of-plane oriented [17]. Consistent with this, we did not observe any shift in the out-of-plane hysteresis, reinforcing the conclusion that there is no detectable exchange bias coupling in our NiO(001)/Co bilayer system. Nonetheless, the enhanced coercivity compared to a single Co layer indicates the presence of interfacial exchange coupling between Co and NiO layers, which affects the magnetization dynamics.

IV. X-RAY SPECTROSCOPY

XMLD measurements were performed with x-ray incidence angles θ of 0° and 60° with respect to the surface normal of the samples [see Fig. 2(a)], allowing us to probe both the in-plane and out-of-plane anisotropies of the AF NiO layer. The XMLD was obtained by subtracting x-ray absorption spectroscopy (XAS) spectra obtained with linear horizontal (lh) and linear vertical (lv) polarized light, using

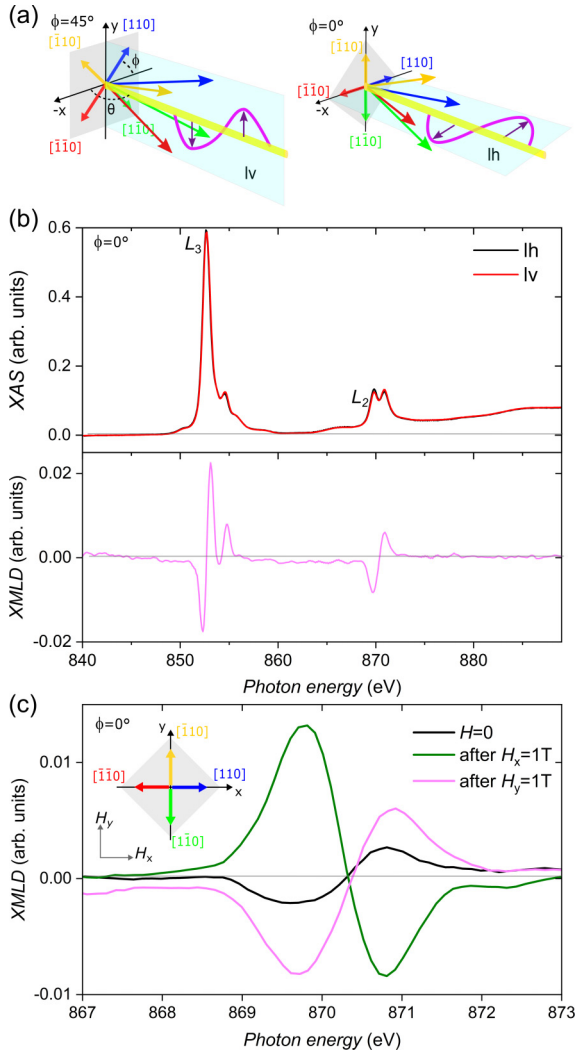

FIG. 2. (a) Schematic illustration of the two experimental geometries ($\phi = 45°$ and $0°$). The azimuthal angle ϕ is defined as the angle between the x axis and the in-plane anisotropic easy axis, while θ represents the x-ray incidence angle with respect to the sample surface normal. At $\theta = 0°$ the linear horizontal (lh) polarization points along the x and the linear vertical (lv) polarization along the y direction. The four easy anisotropy directions of NiO(001) and their in-plane projections are shown in red, green, orange, and blue. (b) XAS and XMLD spectra at the Ni $L_{3,2}$ edges for a sample mounted with its in-plane easy axes aligned parallel to the polarization direction of the x-rays ($\phi = 0°$) after applying a magnetic field along the lv polarization direction. The top panel shows the XAS spectra for both lh (black curve) and lv (red curve) polarizations, while the bottom panel presents the corresponding XMLD spectrum, i.e., the difference between lv and lh, displaying a $-I_{45}$ spectral shape. (c) XMLD spectra at the Ni L_2 edge before (black curve) and after the application of a 1 T magnetic field in the x direction (green curve) and y direction (magenta curve). The spectra reveal an inversion of the XMLD signal after the application of a 1 T magnetic field in the y direction, indicating a reorientation of the Néel vector and confirming the switching of AF domains in the NiO layer. The total electron yield (TEY) signal is shown in the spectra. The inset provides a simplified schematic of the in-plane anisotropy directions only.

total electron yield (TEY) and fluorescence yield (FY) as detection modes. All measurements were carried out at room temperature. Two pieces of the same sample were used, one with the easy anisotropy direction azimuthally rotated by $\phi = 0°$ and one rotated by $\phi = 45°$ with respect to the x direction. Both samples displayed strong XMLD signals at a $\theta = 60°$ incidence angle (see Fig. S7 in [46]), indicating a significant perpendicular component of the spin orientation in the AF NiO layer.

Figure 2(b) presents the XAS and XMLD spectra at $\phi = 0°$ recorded after the application of a magnetic field, using the TEY mode for detection. In octahedral symmetry, the $L_{3,2}$ XMLD exhibits two fundamental spectra, referred to as the I_0 and I_{45} spectra [8,10]. At the L_2 edge, these two spectra share almost identical line shapes but display opposite intensities, making it difficult to distinguish between the I_0 and $-I_{45}$ spectra using only the L_2 XMLD. To resolve this issue, the L_3 XMLD must also be measured, as it features two distinctly different fundamental spectra. An example of the $-I_{45}$ spectrum is shown in Fig. 2(b), with a line shape that aligns well with the data published in the literature [8,10]. For the remainder of this paper, we will only make use of the L_2 region of the XMCD as this allows for a full analysis of the data, while noting that we verified the consistency of the L_3 XMLD.

The main findings are shown in Fig. 2(c): First, the XMLD signal increases after applying a magnetic field in the x direction (green line) compared to the as-grown state (black line). Second, an inversion of the XMLD signal is observed when a magnetic field is applied in the perpendicular y direction (magenta line), indicating a reorientation of the Néel vector.

This distinct behavior of the XMLD was only observed at $\phi = 0°$, as illustrated in Fig. 3. In this figure, the FY signal, recorded simultaneously with the TEY signal, is displayed. Unlike in TEY mode, FY detection enables measurements in the presence of a magnetic field. However, FY has the drawback of producing a noisier signal that is often subject to distortions caused by self-absorption effects [47] as well as having different transition matrix elements [48].

At the normal incidence of the beam ($\theta = 0°$), XMLD was observed only at $\phi = 0°$ [see Fig. 3(a1)], while no XMLD signal was detected at $\phi = 45°$ [see Fig. 3(b1)]. This observation is consistent with previous studies on patterned NiO films, where domains exhibit both out-of-plane and in-plane components, with the in-plane component oriented diagonally in the (001) crystalline plane [17]. A magnetic field of 1 T was then applied in the x direction, which lies in the plane of the sample and is perpendicular to the x-ray beam. Although this field is more than sufficient to saturate the Co layer, it is much too weak to significantly alter the magnetic order of NiO.

In antiferromagnets, the spin structure is primarily governed by exchange coupling due to the absence of dipolar interactions, often requiring magnetic fields on the order of tens of Tesla to induce significant modifications. However, additional factors such as magnetocrystalline anisotropy, magnetoelastic effects, and pinning disorder also influence the stability and dynamics of the spin structure. Notably, studies have shown that domain walls in bulk crystalline NiO can be displaced by moderate magnetic fields ranging from a few

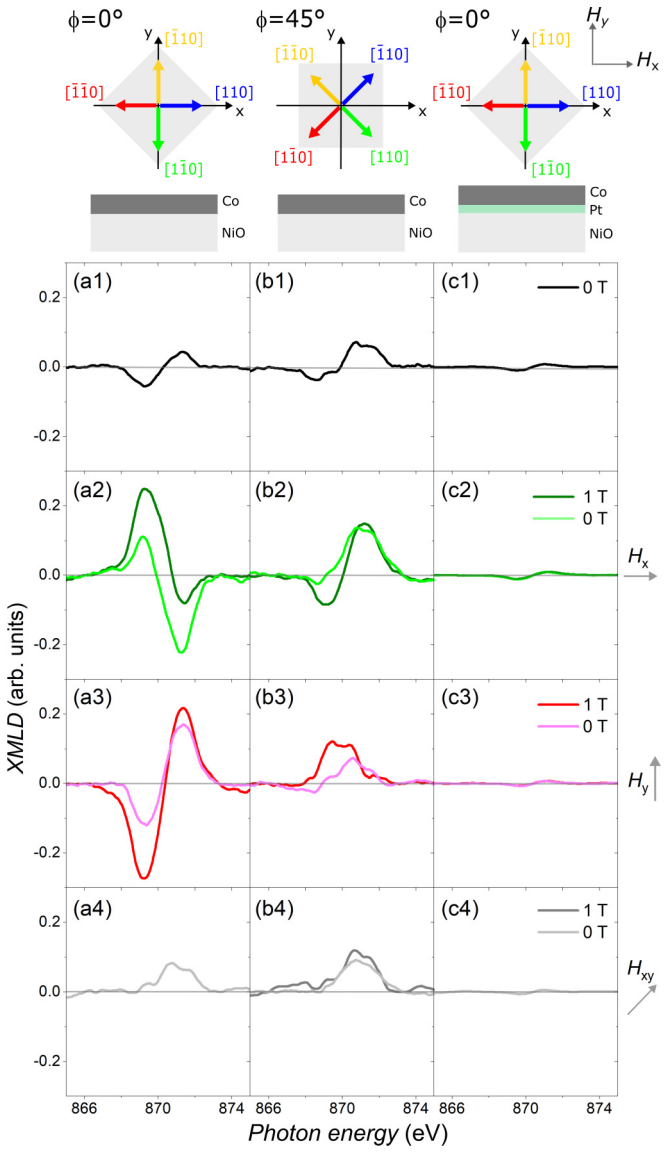

FIG. 3. XMLD spectra at the Ni L_2 edge, measured at room temperature under various applied magnetic fields. The x-rays were incident parallel to the surface normal, and only the fluorescence yield (FY) signal is shown. Panels (a1)–(a4) display XMLD measurements for a sample mounted with its in-plane easy axes aligned parallel to the polarization direction of the x-rays ($\phi = 0°$). The spectra are shown (a1) before applying any magnetic field, (a2) during and after applying a 1 T magnetic field in the x direction, (a3) in the y direction, and (a4) in the diagonal x-y direction. Panels (b1)–(b4) illustrate the same measurements for a sample mounted with the easy axes aligned diagonally relative to the x-ray polarization directions. Panels (c1)–(c4) show the results for a control sample with a 1.5-nm-thick Pt interlayer, which magnetically decouples the NiO and Co layers. This control sample helps to confirm whether the observed inversion and reduction in XMLD is due to interfacial effects between NiO and Co. The direction of the applied magnetic field relative to the sample orientation is indicated by the arrows on the right side of each row of panels. The schematics at the top of the figure illustrate the orientation of the easy anisotropy directions of the AF relative to the magnetic fields and the layer stack for columns (a), (b), and (c). The control sample shown in column (c) has the same orientation as in column (a) ($\phi = 0°$).

hundred mT to a few T [49]. In contrast, reorienting domains in thin films of NiO is typically more challenging due to the pronounced effects of strain, defects, and other forms of disorder, which significantly enhance the pinning of Néel domains. A diverse range of antiferromagnetic behavior is observed in other materials, such as $RFeO_3$ (R = rare earth element), where the canted moment can be flipped along the c axis by a magnetic field as small as 10 mT [50]. Similarly, in other AF insulators such as Cr_2O_3, a spin-flop transition occurs when a field exceeding 6 T is applied along the [001] axis [51]. Despite this, a visible XMLD signal was still observed at $\phi = 0°$, which was slightly reduced but remained detectable after the magnetic field was turned off [see Fig. 3(a2)]. When the same process was repeated with a magnetic field applied in the y direction, a reversal of the XMLD contrast was observed, both while the field was applied and after it was removed [see Fig. 3(a3)].

Both observations can be attributed to a saturation effect of the in-plane component of the AF. Remarkably, a relatively moderate field of only 1 T was sufficient to induce this effect. A field of this strength ensures that the Co layer is saturated [see Fig. 1(c)], but smaller fields are likely to have the same effect. Upon reducing the field to zero, there is a partial reorientation—and likely a randomization—of the in-plane domains of NiO, with a slight predominance of domains still aligned in the direction of the previously applied field. The initial state appeared to be even more, but not completely randomized, as indicated by a much smaller XMLD signal compared to when the fields were applied [see black line in Fig. 3(a1)]. Given that the x-ray beam size is $200 \times 100\,\mu m^2$, the AF domains are likely much smaller than the beam size, allowing sufficient domain averaging to take place. When a magnetic field was applied in the diagonal H_{xy} direction, the XMLD signal was effectively 'erased'—a result of the linear polarization of the x-rays not being sensitive to this direction [see Fig. 3(a4)].

The effect was nearly suppressed at $\phi = 45°$, where both the x and y directions correspond to hard anisotropy directions. In this case, the XMLD signal was only observed while the magnetic field was applied and disappeared once the field was switched off [see Figs. 3(b2) and 3(b3)]. This behavior suggests that the domains relax into one of the easy axis directions when the external field is removed. At this particular sample orientation, all easy axis directions produce the same XMLD contrast, making it impossible to distinguish between them. Unfortunately, our undulator is capable of providing linearly polarized x-rays only between 0° and 90°; however, to perform a more detailed analysis of the relaxed domain states, linear polarization at 135° would be required [10]. As a result, further analysis of the domain relaxation behavior could not be conducted.

Figures 3(c1)–3(c4) show the XMLD spectra for a control sample with a 1.5-nm-thick Pt interlayer between the NiO and Co layers. Since FY is bulk sensitive, the additional Pt interlayer is not expected to significantly attenuate the XMLD signal originating from the buried NiO layer. The smaller XMLD signal [see Fig. 3(c1)] is likely to originate from a greater randomization of the spin structure in NiO in the absence of the Co adlayer. Unlike the samples without the

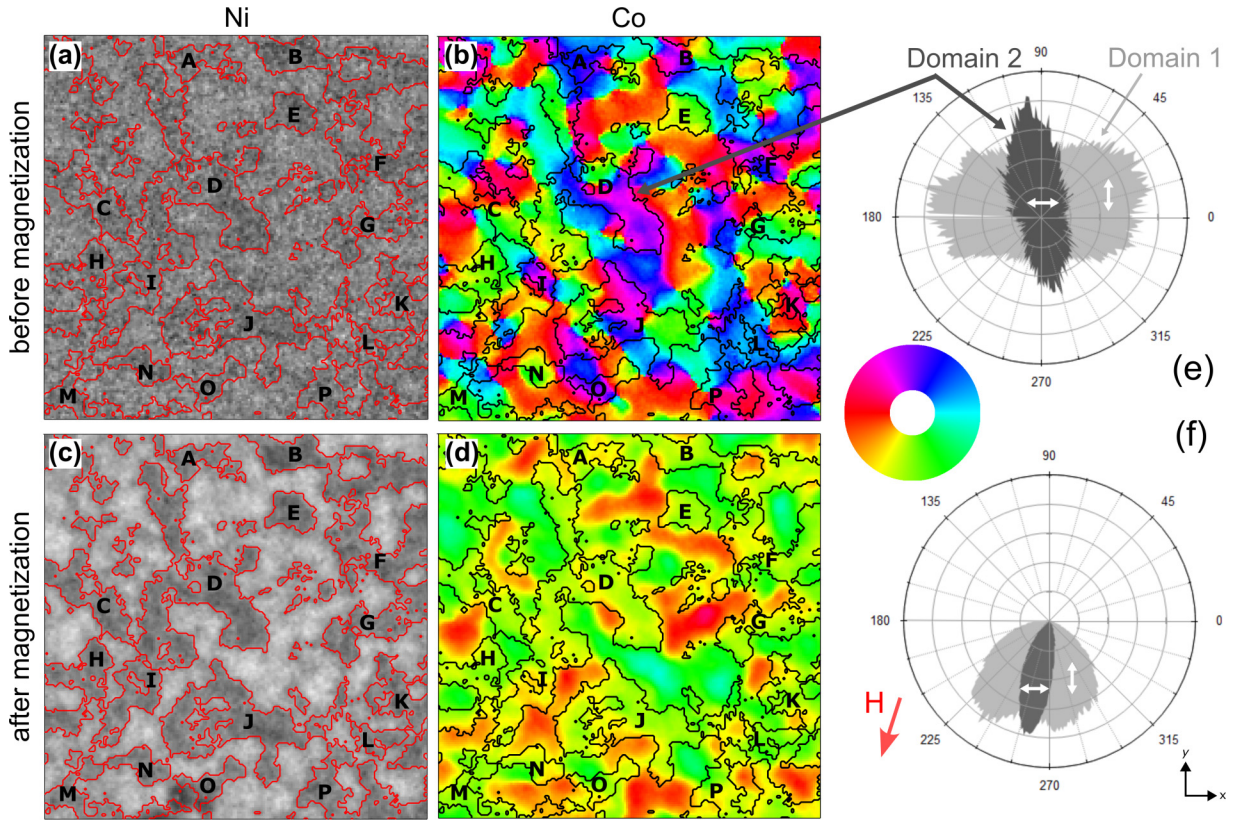

FIG. 4. XMLD-PEEM images of NiO with a field-of-view of $2.4\times2.4\,\mu m^2$ taken at 0° sample rotation, showing the domain structures before and after applying a magnetic field. The field-of-view was 12 μm and a zoom-in of a $2.4\times2.4\,\mu m^2$ area is shown here. (a) XMLD-PEEM image of NiO before the application of a magnetic field, where two types of AF domains are faintly visible, which can be identified via their Néel vectors oriented either vertically (Domain 1) or horizontally (Domain 2). (b) Vector map of the Co magnetization directions before applying a magnetic field, with a color wheel representing the corresponding in-plane magnetization directions. (c) XMLD-PEEM image of NiO after applying a magnetic field. (d) Vector map of Co after the magnetic field application, showing a more uniform distribution of magnetization directions. (e), (f) Polar histograms of the Co magnetization directions corresponding to Domain 1 (light gray) and Domain 2 (dark gray) in NiO, shown (e) before and (f) after the magnetic field application. The red arrow indicates the direction of the applied magnetic field. The red outlines in (a) and (c) highlight the major Domain 2 regions that are already visible before the field is applied, though the domain structure is more complicated in this case. The black outlines in (b) and (d) for Co correspond to the Domain 2 region in NiO, outlined in red in (a) and (c). Capital letters indicate the corresponding Domain 2 regions in panels (a) through (d).

Pt interlayer [see Figs. 3(a1)–3(a4) and 3(b1)–3(b4)], no increase or inversion of the XMLD signal is observed. While the XMLD in remanence is slightly reduced compared to that measured in the applied field, the reduction is significantly smaller and shows no dependence on the direction of the magnetic field. These observations provide strong evidence that the effects observed in the samples without the Pt interlayer are indeed due to interfacial interactions between the NiO and Co layers.

V. DOMAIN IMAGING

To gain deeper insight into the switching processes occurring in the NiO/Co bilayers, the same sample was imaged using photoemission electron microscopy (PEEM) with both XMCD and XMLD effects. The x-ray incidence angle relative to the sample surface was 16°, allowing the probing of both the in-plane and out-of-plane components of the Néel vector. The sample was mounted with an azimuthal angle of $\phi = 0°$ on the sample holder so that the x-ray beam was aligned almost parallel to the easy axis direction of the sample. The out-of-plane component of the Néel vector in NiO(001) is constant and significantly larger than the in-plane component [17]. In the X-PEEM at the I06 beamline at Diamond, the lh x-ray polarization is nearly fully aligned with the out-of-plane component of the Néel vector, dominating the contrast in the images. Contrary to that, the lv polarization is fully aligned in the plane of the sample and is therefore most sensitive to changes in the in-plane component of the Néel vector. Therefore, lv polarization was used for all images in this study to maximize the contrast from in-plane AF domains.

To generate dichroic images, the x-ray energy was varied between the two peaks at the Ni L_2 edge. The dichroic contrast was then calculated using $[I(E_1) - I(E_2)]/[I(E_1) + I(E_2)]$ with $E_1 < E_2$, where $I(E)$ represents the intensity at a given energy. A bright contrast indicates that the in-plane component of the Néel vector is oriented transverse to the x-ray beam, while a dark contrast signifies longitudinal alignment. Hence, in Figs. 4(a) and 4(c), AF domains appear brighter if the in-plane component of the Néel vector is aligned vertically and darker if aligned horizontally. If the sample is rotated by 90° around the surface normal, this contrast reverses, with

vertical components appearing darker than horizontal ones (see Figs. S4(a), S4(b), S5(a) and S5(b) in [46]).

The field-of-view was 12 μm and the domain sizes were of the order of micrometers, much smaller than the beam size used in the x-ray absorption measurements. These measurements covered a sufficiently large number of AF domains, allowing for a statistical interpretation of the results. The consistency of results across multiple sample locations, all showing similar qualitative behavior of XMLD reduction and inversion, confirms that the observations are robust and not due to potential artifacts such as beam drift over large domains. This is supported by repeated experiments under the same conditions, which consistently showed the same trends (see Fig. S1 in [46]).

First, we note that the XMLD contrast appears fainter and more prone to noise in the image taken before magnetization [see Fig. 4(a)], compared to the image acquired after the application of a magnetic field [see Fig. 4(c)]. To accurately determine the number and spatial arrangement of the AF domains, we carried out a principle component analysis (PCA) on the Ni XMLD images [52], which automatically identifies clusters of pixels with the same XMLD spectroscopic footprint. Remarkably, the algorithm identified only two types of AF domains: Domain 1 (Domain 2) with the Néel vector along the y direction (x direction) [see Figs. 4(a) and 4(c)].

Secondly, the FM magnetization in the Co film broadly aligns with the AF domains in the NiO layer. This alignment becomes evident when comparing the outlines of the AF domains, identified through PCA, with the vector maps of the Co magnetization [see Figs. 4(b) and 4(d)]. In Figs. 4(e) and 4(f), the angular distributions of the Co magnetization corresponding to Domain 1 (light gray) and Domain 2 (dark gray) in NiO are shown. For Domain 1, the Co magnetization shows a broad distribution with peaks at 0° and 180°, and troughs at 90° and 270°, indicating a bidirectional alignment along these axes. In contrast, for Domain 2, the Co magnetization is more narrowly concentrated around 100° and 280°, suggesting a more defined alignment direction. The slight misalignment of ∼10° with respect to the vertical direction can be attributed to unintentional rotation during the mounting process of the sample on the PEEM cartridge. Crucially, these results indicate that the spin structure of the Co layer imprints on the NiO layer, with a clear correlation between the orientation of the Néel vector in NiO and the magnetization direction of the Co film.

Third, after saturating in a 1 T magnetic field, the Co magnetization corresponding to Domain 2 aligns exclusively in the direction of the applied field, pointing toward 260° [see Fig. 4(f)]. It is important to highlight that imaging in a 1 T field is not feasible in PEEM due to the distortion of the electron trajectories caused by the Lorentz force. Consequently, all images taken after magnetization were captured in remanence, allowing the Co magnetic moments to relax into potentially different orientations. Given that polycrystalline Co lacks a preferred easy anisotropy direction, this relaxation pattern provides strong evidence for some form of pinning of the Co spins to the AF layer, particularly along the vertical easy anisotropy directions of NiO(001). However, distinguishing whether this behavior is a result of an exchange bias effect or merely an increase in coercivity cannot be determined from PEEM images alone. Hysteresis measurements suggest the latter [see Fig. 1(c)]. Furthermore, the Co magnetization associated with Domain 1 also shows reorientation after magnetization. Notably, the maxima of its angular magnetization distribution are at ∼240° and 280°, which is an approximately 20° offset from the direction of the applied magnetic field and does not align with either the vertical or horizontal easy axis directions of NiO. This observation further supports the notion that the influence of the AF layer on the FM domains is relatively weak, attempting to realign the Co layer in the horizontal direction but only partially succeeding. Another possible explanation is the formation of an exchange spring, where part of the magnetic layers at the interface rotates away from the bulk's equilibrium magnetization direction [53].

From these observations, we conclude that there is no evidence for a strong exchange bias along any of the four easy axis directions of NiO(001). Instead, the increased coercivity observed is more likely due to exchange coupling between the NiO and Co layers without the presence of a unidirectional exchange bias effect.

Finally, we compared the expected XMLD, estimated from the AF domain images, with the measured XMLD from the x-ray spectroscopy data. After applying a magnetic field, 63% of the visible sample area is found in the Domain 1 state, while 37% is in the Domain 2 state. This represents a difference of 26% points, which suggests a reduction by roughly a quarter when compared to a fully saturated or homogeneous domain state in either Domain 1 or 2. This is consistent with the measured XMLD shown in Fig. 3(a), particularly when considering the area under the L_2 edge. For example, the XMLD ratios in and after a 1 T magnetic field are 29% and 33% when applied in the x and y direction, respectively. For this analysis, the area below the first half of the L_2 edge was integrated, which can be either a peak or a trough. This analysis assumes that the AF domains are fully saturated in a 1 T magnetic field. When considering the integration of both the peak and trough of the L_2 edge, slightly higher ratios are obtained.

The inversion of the XMLD signal when changing the direction of the magnetic field aligns well with a reorientation of the AF domains, suggesting that the Co layer exerts a significant influence on the NiO domains rather than the reverse. This highlights the strong coupling between the AF and FM layers and confirms that the observed changes in XMLD are primarily driven by the magnetization dynamics of the Co layer affecting the AF spin structure of NiO.

VI. DISCUSSION

The application of a magnetic field significantly affects both the XMLD spectra and the contrast observed in the NiO XMLD-PEEM images. After applying a magnetic field, the XMLD spectra show a marked increase in intensity, and two distinct types of domains become clearly visible in the XMLD-PEEM images. In contrast, in the as-grown state—prior to applying the magnetic field—the XMLD spectra and AF domains are only faintly distinguishable. This change is unlikely to be caused by any structural alterations of the material due to the applied magnetic field; instead, it suggests a change in the magnetic properties of the NiO layer. One possible explanation is that the AF domains are not uniformly

aligned after growth, and the magnetic field induces a realignment of these domains.

Our findings indicate that a single layer of NiO is resistant to the same in-plane magnetic fields of 1 T (see Fig. S3 in [46]), highlighting the crucial role of the Co adlayer in mediating the control over the AF spin structure via magnetic fields. The canting of NiO toward Fe spins due to exchange coupling was reported by Matsuyama *et al.* [54]. Similarly, antiferromagnetic CoO was shown to be rotatable below a critical thickness when coupled with a ferromagnetic Fe layer [55]. The Néel vector of MnAu was found to reorient in response to the magnetization direction of an adjacent Py layer [56]. Additionally, the imprint of complex spin structures from ferromagnets into antiferromagnets has been reported in patterned thin films, such as vortices in IrMn/Py [57] and CoO/Fe [58], as well as skyrmions in IrMn/Py [59].

The toy model illustrated in Fig. 5 provides a framework for understanding the processes that occur when a magnetic field is applied. In this toy model, the NiO layer consists of stable and unstable AF domains. A magnetic field strong enough to saturate the Co layer aligns the interfacial NiO layer perpendicularly to the Co magnetization. This behavior is attributed to the perpendicular coupling between Co and NiO, consistent with prior x-ray imaging studies [8,10].

However, while the interfacial AF domains rotate under the influence of the field, the bulk of the stable AF domains remain largely unaffected, overall appearing to behave like an antiferromagnetic exchange spring [53]. The unstable AF domains, in contrast, align with the interfacial layer, losing their initial magnetic orientation. Upon removal of the magnetic field, the unstable AF domains retain their new orientation, while the stable AF domains revert to their original state, pulling the Co layer back into its initial alignment. In this simplified toy model, a pattern of perpendicularly aligned AF domains emerges. However, in our experiments, the Co domains are not perfectly perpendicular but exhibit some canting. Nonetheless, we observe two regions that correspond to the two AF domain types in NiO, which are aligned antiparallel to each other.

No clear evidence for an exchange bias effect was obtained either by hysteresis measurements or by the combined XMLD/XMCD imaging study. However, indications of a reciprocal effect are present, where the NiO layer couples to the Co and, at least partially, aligns with its magnetization direction. This interplay underscores the complex magnetic interactions at the NiO/Co interface and highlights the potential of using FM adlayers to manipulate AF spin structures.

The key to understanding this behavior lies in the interfacial exchange coupling and the relative energetics of domain wall formation versus the reorientation of spins in the NiO layer. In our system, the Co layer provides a strong interfacial exchange field that acts directly on the adjacent NiO layer. While NiO spins are generally more stable due to the strong exchange interaction and anisotropy, the interfacial coupling preferentially affects unpinned or weakly pinned NiO domains. These domains are more susceptible to reorientation because the energy required to reorient them or to form a partial exchange spring is lower than the energy needed to nucleate or propagate domain walls in the Co layer. At the interface, the Co spins experience a combined effect of the external magnetic field and the interfacial exchange coupling, which biases their alignment and drives their reorientation in response to the field. Dynamically coupled to the Co spins, the unpinned NiO domains effectively 'follow' this motion. Crucially, the energy landscape within the NiO layer is not uniform: While strongly pinned domains remain largely unaffected, weakly pinned or unstable domains are more easily influenced by the Co magnetization. This selective response

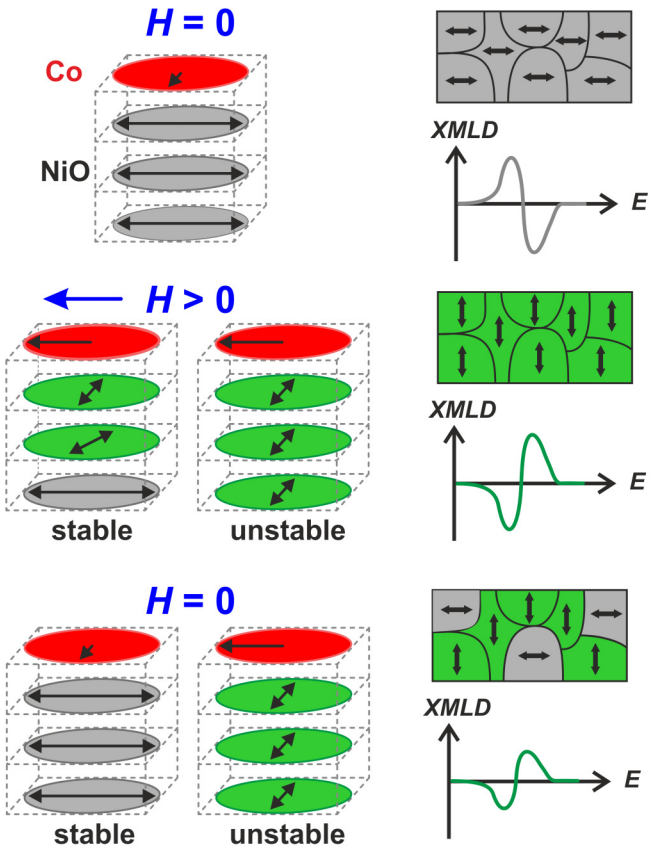

FIG. 5. Toy model illustrating the magnetic reorientation of NiO domains under the influence of a magnetic field applied to the Co adlayer. The NiO layer is conceptually divided into two types of domains: stable and unstable AF domains. When a moderate magnetic field (1 T) is applied, it saturates the Co layer, causing the interfacial NiO layer to align perpendicularly relative to the Co magnetization due to strong perpendicular coupling at the interface. In this process, the unstable AF domains in the NiO layer, which are weakly pinned, follow the Co magnetization and rotate, losing their initial orientation. Conversely, the stable AF domains, which are more rigidly pinned, remain largely unaffected by the field and behave like an exchange spring, only partially responding to the external magnetic field. After the field is removed, the unstable AF domains retain their new alignment while the stable AF domains unwind back to their original orientation, dragging the Co layer with them. This leads to the formation of a mixed domain structure with canted rather than perfectly perpendicular alignment, reflecting the observed behavior in XMLD-PEEM imaging. The toy model explains the absence of a typical exchange bias effect and suggests a reciprocal coupling mechanism where both the NiO and Co layers influence each other's magnetic states.

can result in an observable reorientation of the Néel vector in the NiO layer, while the Co spins themselves are more readily influenced by the applied magnetic field.

Finally, we consider the possibility that the NiO layer may be too thin to establish the strong exchange bias coupling typically observed in similar systems. While a systematic thickness dependence to determine the onset of exchange bias or changes in coercivity was not performed, the thickness of the NiO layer was measured using XRR [see Fig. 1(d)]. The measured thickness of 23 nm is significantly larger than the critical thicknesses reported in the literature [12–14,60,61]. Based on this measurement, we can exclude suppressed exchange coupling at the interface as the origin of the observed phenomena.

VII. SUMMARY & CONCLUSIONS

Our study provided several new insights into the behavior of the NiO/Co system. First, the Ni-XMLD spectra of NiO(001)/Co are more pronounced in a magnetic field compared to a zero field. This observation is based on measurements using FY, which is unaffected by magnetic fields, as demonstrated in Figs. 3(a2) and 3(a3). Second, XMLD-PEEM images at the Ni L_2 edge show two distinct domain types, as seen in Fig. 4. After applying a magnetic field, a surplus of 26% of one domain type over the other was observed, consistent with spectroscopy data showing a residual XMLD signal after the field was removed, as illustrated in Figs. 3(a2) and 4(c). Third, the hysteresis measurements reveal that the remanence is reduced compared to saturation, which agrees with the canting of Co toward NiO in regions corresponding to one of the domain types. This relationship is highlighted in the red and blue regions of Fig. 4(d) and corroborated by Fig. 1(c). Finally, and most importantly, the Ni-XMLD spectra invert when the magnetic field is applied along perpendicular directions corresponding to the easy axis anisotropy directions, as shown in Fig. 2(c) and Figs. 3(a2) and 3(a3). However, direct imaging of the NiO spin state under a magnetic field is not feasible using XMLD-PEEM, as the field deflects the secondary electrons generated by the x-rays, complicating image acquisition.

In summary, we have demonstrated the effective manipulation of the AF domain orientation in NiO thin films through the application of moderate magnetic fields of only 1 T. This control is achieved by utilizing a thin FM Co adlayer that shares an interface with the NiO layer. The exchange coupling between the Co and NiO layers facilitates the reorientation of the AF spin structure, which would otherwise be highly resistant to external magnetic fields.

Our findings show that the NiO layer, when in contact with the Co adlayer, partially follows the magnetization direction of the Co under an applied magnetic field, leading to significant changes in the spin structure. The use of XMLD spectroscopy has allowed us to directly observe the inversion of XMLD signals, indicating a reorientation of the Néel vector in NiO. This result is further corroborated by XMLD-PEEM imaging, which reveals a direct correlation between the FM and AF domains at the interface. PCA of these images provides deeper insights into the complex interplay between the stable and unstable AF domains and their response to the applied magnetic fields. Our study establishes that the presence of a ferromagnetic adlayer can effectively act as a 'magnetic lever' to manipulate the AF spin structure in thin films, opening up new avenues for AF spintronics. The ability to control the AF spin orientation with such precision and moderate fields makes this approach highly promising for the development of AF-based devices with enhanced robustness against external magnetic perturbations and faster switching speeds.

ACKNOWLEDGMENTS

E.H. acknowledges a Science and Technology Facilities Council (STFC)-Diamond Light Source-Engineering and Physical Sciences Research Council (EPSRC) studentship (No. EP/R513295/1 and No. EP/T517811/1). We would like to thank Dr. Gavin Stenning and Dr. Daniel Nye for help on the x-ray diffractometer instrument in the Materials Characterisation Laboratory at the ISIS Neutron and Muon Source. We thank Diamond Light Source for the provision of beamtime on beamline I06 under proposal NR35404 and for access to the facilities of the Materials Characterisation Laboratory.

[1] X. Marti, I. Fina, C. Frontera, J. Liu, P. Wadley, Q. He, R. J. Paull, J. D. Clarkson, J. Kudrnovský, I. Turek, J. Kuneš, D. Yi, J.-H. Chu, C. T. Nelson, L. You, E. Arenholz, S. Salahuddin, J. Fontcuberta, T. Jungwirth, and R. Ramesh, Room-temperature antiferromagnetic memory resistor, Nat. Mater. **13**, 367 (2014).

[2] T. Jungwirth, X. Marti, P. Wadley, and J. Wunderlich, Antiferromagnetic spintronics, Nat. Nanotechnol. **11**, 231 (2016).

[3] J. Železný, P. Wadley, K. Olejník, A. Hoffmann, and H. Ohno, Spin transport and spin torque in antiferromagnetic devices, Nat. Phys. **14**, 220 (2018).

[4] J. Stöhr, A. Scholl, T. J. Regan, S. Anders, J. Lüning, M. R. Scheinfein, H. A. Padmore, and R. L. White, Images of the antiferromagnetic structure of a NiO(100) surface by means of x-ray magnetic linear dichroism spectromicroscopy, Phys. Rev. Lett. **83**, 1862 (1999).

[5] H. Ohldag, A. Scholl, F. Nolting, S. Anders, F. U. Hillebrecht, and J. Stöhr, Spin reorientation at the antiferromagnetic NiO(001) surface in response to an adjacent ferromagnet, Phys. Rev. Lett. **86**, 2878 (2001).

[6] E. Arenholz, G. van der Laan, and F. Nolting, Magnetic structure near the CoNiO (001) interface, Appl. Phys. Lett. **93**, 162506 (2008).

[7] M. Finazzi, A. Brambilla, P. Biagioni, J. Graf, G. H. Gweon, A. Scholl, A. Lanzara, and L. Duò, Interface coupling transition in a thin epitaxial antiferromagnetic film interacting with a ferromagnetic substrate, Phys. Rev. Lett. **97**, 097202 (2006).

[8] G. van der Laan, N. D. Telling, A. Potenza, S. S. Dhesi, and E. Arenholz, Anisotropic x-ray magnetic linear dichroism and spectromicroscopy of interfacial Co/NiO(001), Phys. Rev. B **83**, 064409 (2011).

[9] J. Li, A. Tan, K. W. Moon, A. Doran, M. A. Marcus, A. T. Young, E. Arenholz, S. Ma, R. F. Yang, C. Hwang, and Z. Q. Qiu, Imprinting antivortex states from ferromagnetic Fe into antiferromagnetic NiO in epitaxial NiO/Fe/Ag(001) microstructures, Appl. Phys. Lett. **104**, 112407 (2014).

[10] E. Arenholz, G. van der Laan, R. V. Chopdekar, and Y. Suzuki, Angle-dependent Ni^{2+} X-ray magnetic linear dichroism: Interfacial coupling revisited, Phys. Rev. Lett. **98**, 197201 (2007).

[11] H. Ohldag, G. van der Laan, and E. Arenholz, Correlation of crystallographic and magnetic domains at Co/NiO(001) interfaces, Phys. Rev. B **79**, 052403 (2009).

[12] Y. J. Zhang, L. Wu, J. Ma, Q. H. Zhang, A. Fujimori, J. Ma, Y. H. Lin, C. W. Nan, and N. X. Sun, Interfacial orbital preferential occupation induced controllable uniaxial magnetic anisotropy observed in Ni/NiO(110) heterostructures, npj Quant. Mater. **2**, 17 (2017).

[13] K. Amemiya and M. Sakamaki, Manipulation of magnetic properties of ferromagnetic Ni thin films grown on Cu(001) by antiferromagnetic NiO and effects of voltage application, Jpn. J. Appl. Phys. **57**, 0902B3 (2018).

[14] S. Kobayashi, H. Koizumi, H. Yanagihara, J. Okabayashi, T. Kondo, T. Kubota, K. Takanashi, and Y. Sonobe, Perpendicular magnetic anisotropy of an ultrathin Fe layer grown on NiO(001), Phys. Rev. Appl. **19**, 064005 (2023).

[15] T. Moriyama, K. Oda, T. Ohkochi, M. Kimata, and T. Ono, Spin torque control of antiferromagnetic moments in NiO, Sci. Rep. **8**, 14167 (2018).

[16] L. Baldrati, O. Gomonay, A. Ross, M. Filianina, R. Lebrun, R. Ramos, C. Leveille, F. Fuhrmann, T. R. Forrest, F. Maccherozzi, S. Valencia, F. Kronast, E. Saitoh, J. Sinova, and M. Kläui, Mechanism of Neél order switching in antiferromagnetic thin films revealed by magnetotransport and direct imaging, Phys. Rev. Lett. **123**, 177201 (2019).

[17] C. Schmitt, L. Baldrati, L. Sanchez-Tejerina, F. Schreiber, A. Ross, M. Filianina, S. Ding, F. Fuhrmann, R. Ramos, F. Maccherozzi, D. Backes, M. A. Mawass, F. Kronast, S. Valencia, E. Saitoh, G. Finocchio, and M. Kläui, Identification of Neél vector orientation in antiferromagnetic domains switched by currents in NiO/Pt thin films, Phys. Rev. Appl. **15**, 034047 (2021).

[18] M. Ślęzak, H. Nayyef, P. Drozdz, W. Janus, A. Koziol-Rachwal, M. Szpytma, M. Zajac, T. O. Mentes, F. Genuzio, A. Locatelli, and T. Slezak, Controllable magnetic anisotropy and spin orientation of a prototypical easy-plane antiferromagnet on a ferromagnetic support, Phys. Rev. B **104**, 134434 (2021).

[19] H. Meer, O. Gomonay, C. Schmitt, R. Ramos, L. Schnitzspan, F. Kronast, M. A. Mawass, S. Valencia, E. Saitoh, J. Sinova, L. Baldrati, and M. Kläui, Strain-induced shape anisotropy in antiferromagnetic structures, Phys. Rev. B **106**, 094430 (2022).

[20] H. Meer, S. Wust, C. Schmitt, P. Herrgen, F. Fuhrmann, S. Hirtle, B. Bednarz, A. Rajan, R. Ramos, M. A. Niño, M. Foerster, F. Kronast, A. Kleibert, B. Rethfeld, E. Saitoh, B. Stadtmüller, M. Aeschlimann, and M. Kläui, Laser-induced creation of antiferromagnetic 180° domains in NiO/Pt bilayers, Adv. Funct. Mater. **33**, 2213536 (2023).

[21] W. Janus, T. Slezak, M. Slezak, M. Szpytma, P. Drozdz, H. Nayyef, A. Mandziak, D. Wilgocka-Slezak, M. Zajac, M. Jugovac, T. O. Mentes, A. Locatelli, and A. Koziol-Rachwal, Tunable magnetic anisotropy of antiferromagnetic NiO in (Fe)/NiO/MgO/Cr/MgO(001) epitaxial multilayers, Sci. Rep. **13**, 4824 (2023).

[22] C. Schmitt, L. Sanchez-Tejerina, M. Filianina, F. Fuhrmann, H. Meer, R. Ramos, F. Maccherozzi, D. Backes, E. Saitoh, G. Finocchio, L. Baldrati, and M. Kläui, Identifying the domain-wall spin structure in antiferromagnetic NiO/Pt, Phys. Rev. B **107**, 184417 (2023).

[23] T. Moriyama, L. Sanchez-Tejerina, K. Oda, T. Ohkochi, M. Kimata, Y. Shiota, H. Nojiri, G. Finocchio, and T. Ono, Micromagnetic understanding of evolutions of antiferromagnetic domains in NiO, Phys. Rev. Mater. **7**, 054401 (2023).

[24] T. Bhowmick, S. K. Jerng, J. H. Jeon, S. B. Roy, Y. H. Kim, J. Seo, J. S. Kim, and S. H. Chun, Suppressed weak antilocalization in the topological insulator Bi_2Se_3 proximity coupled to antiferromagnetic NiO, Nanoscale **9**, 844 (2017).

[25] J. Fischer, O. Gomonay, R. Schlitz, K. Ganzhorn, N. Vlietstra, M. Althammer, H. Huebl, M. Opel, R. Gross, S. T. B. Goennenwein, and S. Geprägs, Spin Hall magnetoresistance in antiferromagnet/heavy-metal heterostructures, Phys. Rev. B **97**, 014417 (2018).

[26] H. Wang, J. Finley, P. Zhang, J. Han, J. T. Hou, and L. Liu, Spin-orbit-torque switching mediated by an antiferromagnetic insulator, Phys. Rev. Appl. **11**, 044070 (2019).

[27] C. C. Chiang, S. Y. Huang, D. Qu, P. H. Wu, and C. L. Chien, Absence of evidence of electrical switching of the antiferromagnetic Néel vector, Phys. Rev. Lett. **123**, 227203 (2019).

[28] Y. Hui, Y. Zhang, Y. Q. Wang, X. Gan, L. Wang, S. Liu, J. Zhang, Y. Hao, and H. H. Ma, Room-temperature anomalous inverse spin Hall effect in an easy-plane antiferromagnetic insulator for Néel-vector manipulation and detection, Phys. Rev. Appl. **18**, 034032 (2022).

[29] D. Zhu, T. Zhang, X. Fu, R. Hao, A. Hamzić, H. Yang, X. Zhang, H. Zhang, A. Du, D. Xiong, K. Shi, S. Yan, S. Zhang, A. Fert, and W. Zhao, Sign change of spin-orbit torque in Pt/NiO/CoFeB structures, Phys. Rev. Lett. **128**, 217702 (2022).

[30] X. Z. Chen, R. Zarzuela, J. Zhang, C. Song, X. F. Zhou, G. Y. Shi, F. Li, H. A. Zhou, W. J. Jiang, F. Pan, and Y. Tserkovnyak, Antidamping-torque-induced switching in biaxial antiferromagnetic insulators, Phys. Rev. Lett. **120**, 207204 (2018).

[31] M. Y. Yan, J. M. Yan, M. Y. Zhang, T. W. Chen, G. Y. Gao, F. F. Wang, Y. Chai, and R. K. Zheng, Nonvolatile manipulation of electronic and ferromagnetic properties of NiO-Ni epitaxial film by ferroelectric polarization charge, Appl. Phys. Lett. **117**, 232901 (2020).

[32] Y. J. Zhang, J. H. Chen, L. L. Li, J. Ma, C. W. Nan, and Y. H. Lin, Ferroelectric strain modulation of antiferromagnetic moments in Ni/NiO ferromagnet/antiferromagnet heterostructures, Phys. Rev. B **95**, 174420 (2017).

[33] J. C. Loudon, Antiferromagnetism in NiO observed by transmission electron diffraction, Phys. Rev. Lett. **109**, 267204 (2012).

[34] I. Gray, T. Moriyama, N. Sivadas, G. M. Stiehl, J. T. Heron, R. Need, B. J. Kirby, D. H. Low, K. C. Nowack, D. G. Schlom, D. C. Ralph, T. Ono, and G. D. Fuchs, Spin seebeck imaging of spin-torque switching in antiferromagnetic Pt/NiO heterostructures, Phys. Rev. X **9**, 041016 (2019).

[35] H. Qiu, L. Zhou, C. Zhang, J. Wu, Y. Tian, S. Cheng, S. Mi, H. Zhao, Q. Zhang, D. Wu, B. Jin, J. Chen, and P. Wu, Ultrafast

spin current generated from an antiferromagnet, Nat. Phys. **17**, 388 (2021).

[36] E. Rongione, O. Gueckstock, M. Mattern, O. Gomonay, H. Meer, C. Schmitt, R. Ramos, T. Kikkawa, M. Mičica, E. Saitoh, J. Sinova, H. Jaffrès, J. Mangeney, S. T. B. Goennenwein, S. Geprägs, T. Kampfrath, M. Kläui, M. Bargheer, T. S. Seifert, S. Dhillon *et al.*, Emission of coherent THz magnons in an antiferromagnetic insulator triggered by ultrafast spin–phonon interactions, Nat. Commun. **14**, 1818 (2023).

[37] D. Yang, W. Wen, C. Xu, K. Lee, T. Yu, and H. Yang, Electrically tunable terahertz resonance in antiferromagnetic nio/pt heterostructures, Phys. Rev. Appl. **20**, 014023 (2023).

[38] X. Wang, R. Y. Engel, I. Vaskivskyi, D. Turenne, V. Shokeen, A. Yaroslavtsev, O. Granäs, R. Knut, J. O. Schunck, S. Dziarzhytski, G. Brenner, R. P. Wang, M. Kuhlmann, F. Kuschewski, W. Bronsch, C. Schüssler-Langeheine, A. Styervoyedov, S. S. P. Parkin, F. Parmigiani, O. Eriksson *et al.*, Ultrafast manipulation of the NiO antiferromagnetic order via sub-gap optical excitation, Faraday Discuss. **237**, 300 (2022).

[39] C. Y. Liu, K. Ruotsalainen, K. Bauer, R. Decker, A. Pietzsch, and A. Föhlisch, Excited-state exchange interaction in NiO determined by high-resolution resonant inelastic X-ray scattering at the Ni $M_{2,3}$ edges, Phys. Rev. B **106**, 035104 (2022).

[40] M. Dąbrowski, T. Nakano, D. M. Burn, A. Frisk, D. G. Newman, C. Klewe, Q. Li, M. Yang, P. Shafer, E. Arenholz, T. Hesjedal, G. van der Laan, Z. Q. Qiu, and R. J. Hicken, Coherent transfer of spin angular momentum by evanescent spin waves within antiferromagnetic NiO, Phys. Rev. Lett. **124**, 217201 (2020).

[41] D. Alders, T. Hibma, G. Sawatzky, K. Cheung, G. van Dorssen, H. Padmore, M. Roper, G. van der Laan, J. Vogel, and M. Sacchi, Grazing incidence reflectivity and total electron yield effects in soft x-ray absorption spectroscopy, J. Appl. Phys. **82**, 3120 (1997).

[42] G. van der Laan, Study of antiferromagnetic NiO using grazing incidence reflectivity and soft x-ray absorption, J. Magn. Magn. Mater. **192**, 297 (1999).

[43] P. Kienzle, J. Krycka, N. Patel, and I. Sahin, Refl1D (Version 0.8.16) [Computer Software]. College Park, MD: University of Maryland. Retrieved Jan 05, 2024.

[44] J. Nogués and I. K. Schuller, Exchange bias, J. Magn. Magn. Mater. **192**, 203 (1999).

[45] A. Berkowitz and K. Takano, Exchange anisotropy—a review, J. Magn. Magn. Mater. **200**, 552 (1999).

[46] See Supplemental Material at http://link.aps.org/supplemental/10.1103/PhysRevMaterials.9.014408 for the investigation of potential training effects, the homogeneity of the sample, a single NiO layer, and dichroic images for which the sample was rotated by 90°.

[47] S. Eisebitt, T. Boske, J.-E. Rubensson, and W. Eberhardt, Determination of absorption coefficients for concentrated samples by fluorescence detection, Phys. Rev. B **47**, 14103 (1993).

[48] G. van der Laan and A. Figueroa, X-ray magnetic circular dichroism-a versatile tool to study magnetism, Coord. Chem. Rev. **277-278**, 95 (2014).

[49] H. Kondoh and T. Takeda, Observation of antiferromagnetic domains in Nickel oxide, J. Phys. Soc. Jpn. **19**, 2041 (1964).

[50] J. S. Zhou, L. G. Marshall, Z. Y. Li, X. Li, and J. M. He, Weak ferromagnetism in perovskite oxides, Phys. Rev. B **102**, 104420 (2020).

[51] S. Seki, T. Ideue, M. Kubota, Y. Kozuka, R. Takagi, M. Nakamura, Y. Kaneko, M. Kawasaki, and Y. Tokura, Thermal generation of spin current in an antiferromagnet, Phys. Rev. Lett. **115**, 266601 (2015).

[52] I. T. Jolliffe and J. Cadima, Principal component analysis: a review and recent developments, Philos. Trans. A Math. Phys. Eng. Sci. **374**, 202 (2016).

[53] A. Scholl, M. Liberati, E. Arenholz, H. Ohldag, and J. Stöhr, Creation of an antiferromagnetic exchange spring, Phys. Rev. Lett. **92**, 247201 (2004).

[54] H. Matsuyama, C. Haginoya, and K. Koike, Microscopic imaging of Fe magnetic domains exchange coupled with those in a NiO(001) surface, Phys. Rev. Lett. **85**, 646 (2000).

[55] J. Wu, J. S. Park, W. Kim, E. Arenholz, M. Liberati, A. Scholl, Y. Z. Wu, C. Hwang, and Z. Q. Qiu, Direct measurement of rotatable and frozen CoO spins in exchange bias system of CoO/Fe/Ag(001), Phys. Rev. Lett. **104**, 217204 (2010).

[56] S. P. Bommanaboyena, D. Backes, L. S. Veiga, S. S. Dhesi, Y. R. Niu, B. Sarpi, T. Denneulin, A. Kovács, T. Mashoff, O. Gomonay, J. Sinova, K. Everschor-Sitte, D. Schönke, R. M. Reeve, M. Kläui, H. J. Elmers, and M. Jourdan, Readout of an antiferromagnetic spintronics system by strong exchange coupling of Mn_2Au and Permalloy, Nat. Commun. **12**, 6539 (2021).

[57] J. Sort, K. S. Buchanan, V. Novosad, A. Hoffmann, G. Salazar-Alvarez, A. Bollero, M. D. Baró, B. Dieny, and J. Nogués, Imprinting vortices into antiferromagnets, Phys. Rev. Lett. **97**, 067201 (2006).

[58] J. Wu, D. Carlton, J. S. Park, Y. Meng, E. Arenholz, A. Doran, A. T. Young, A. Scholl, C. Hwang, H. W. Zhao, J. Bokor, and Z. Q. Qiu, Direct observation of imprinted antiferromagnetic vortex states in CoO/Fe/Ag(001) discs, Nat. Phys. **7**, 303 (2011).

[59] K. G. Rana, R. L. Seeger, S. Ruiz-Gómez, R. Juge, Q. Zhang, K. Bairagi, V. T. Pham, M. Belmeguenai, S. Auffret, M. Foerster, L. Aballe, G. Gaudin, V. Baltz, and O. Boulle, Imprint from ferromagnetic skyrmions in an antiferromagnet via exchange bias, Appl. Phys. Lett. **119**, 192407 (2021).

[60] P. Luches, S. Benedetti, A. D. Bona, and S. Valeri, Magnetic couplings and exchange bias in Fe/NiO epitaxial layers, Phys. Rev. B **81**, 054431 (2010).

[61] J. Xu, C. Zhou, M. Jia, D. Shi, C. Liu, H. Chen, G. Chen, G. Zhang, Y. Liang, J. Li, W. Zhang, and Y. Wu, Imaging antiferromagnetic domains in Nickel oxide thin films by optical birefringence effect, Phys. Rev. B **100**, 134413 (2019).